I

UNITED STATES ATOMIC ENERGY COMMISSION

NDA-15C-40

DISTRIBUTION OF FISSION NEUTRONS IN WATER AT THE INDIUM RESONANCE ENERGY

By
J. Certaine
R. Aronson

June 15, 1954

Nuclear Development Associates, Inc.
White Plains, New York

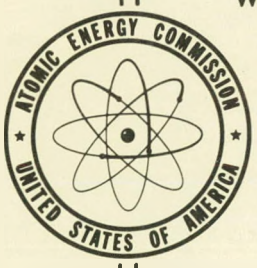

Technical Information Service, Oak Ridge, Tennessee

II

Subject Category, PHYSICS.
Work performed under Contract No. AT(30-1)862.

Project Leader: Herbert Goldstein

ABSTRACT

Calculations have been made by the moment method of the neutron flux distribution at 2.03 ev from a point isotropic fission source in water. Comparison has been made with flux measurements by Hill, Roberts, and Fitch at the indium resonance energy (~1.44 ev). The shapes of the two flux curves agree beyond 10 cm. However, the maximum of the theoretical flux curve is ~5 cm from the origin while the experimental maximum is ~7.5 cm away. The age, defined herein as $r^2/6$ (r being the distance from the origin), is calculated to be 26 cm^2, compared to a measured value of 31 cm^2.

NDA 15C-40

Distribution of Fission Neutrons in Water At the Indium Resonance Energy

J. Certaine
R. Aronson

Measurements of the neutron flux distribution in water from an assumed point isotropic source of fission neutrons have been made by Hill, Roberts, and Fitch using indium foil detectors.(1) The nominal energy of the measured flux was the indium resonance energy, 1.44 ev. We present here theoretical results of calculations of the flux distribution of 2.03 ev neutrons in water arising from a point isotropic fission spectrum source.

The fission spectrum S(E) was represented by Watt's formula

$$S(E) = \sqrt{\frac{2}{\pi e}}\ e^{-E} \sinh\sqrt{2E}\ ,$$

where E is the neutron energy in Mev. The shape of the distribution is expected to be the same at 1.44 ev and at 2.03 ev. The experimental and theoretical results for the flux turn out to be in good agreement except at small penetrations, where there are significant discrepancies.

The behavior of the neutrons is given by the Boltzmann equation. At 2 ev both the molecular binding of the hydrogen and oxygen nuclei and the thermal motion of the molecules can be neglected. The neutrons were assumed to be attenuated by scattering in free hydrogen and oxygen and to be absorbed as well as scattered by oxygen at higher energies, all nuclei taken to be at rest. Degradation of the neutron energy on collision with oxygen nuclei was ignored. A discussion of the data used is given in Appendix I.

The calculation was done by the moment method and is described in Appendix II.

The neutron flux density $F_o(r)$ was computed as a function of the penetration r. The averages $\overline{r^{2n}}$, defined as

$$\overline{r^{2n}} = \frac{\int_0^\infty r^{2n} F_o(r)\, 4\pi r^2\, dr}{\int_0^\infty F_o(r)\, 4\pi r^2\, dr}$$

were also computed.

In the experiment described above $F_o(r)$ was measured (to within a constant factor) out to 92 cm and extrapolated beyond that and $\overline{r^2}$, $\overline{r^4}$, $\overline{r^6}$, and $\overline{r^8}$ computed. To be compared with these quantities are, respectively, the shape of $F_o(r)$ and the values of $\overline{r^2}$, $\overline{r^4}$, $\overline{r^6}$, and $\overline{r^8}$, as computed from the Boltzmann equation.

Figure 1 shows $4\pi r^2 F_o(r)$ as found experimentally and as computed theoretically for a source strength of 1 neutron/sec, the experimental flux being arbitrarily normalized to the same value as the theoretical flux at 20 cm. The same comparison is made in Table I. The agreement is quite good except near the origin. At large penetrations the slope of the theoretical curve appears to be very slightly less than the slope of the experimental curve.*

Comparisons of the experimental and theoretical values of $\overline{r^{2n}}$ and $(\overline{r^{2n}})^{1/2n}$ are given in Table II for n = 1,2,3, and 4.

Of particular interest is the so-called "age" of the indium resonance neutrons, which we will define by the quantity $\overline{r^2}/6$. An experimental age of 31 cm^2 is found as against a theoretical value of 26 cm^2. The fact that the theory gives a smaller result for the age than does the experiment is evidenced in the curves in Figure 1. $\overline{r^2}$ is a measure of the flux fairly near ($r \sim 5$-35 cm) the origin, and the smaller theoretical value is merely a consequence of the fact that the maximum of the theoretical curve is closer to the origin.

---

* A less accurate reconstruction of the theoretical flux based on the first four moments only is presented in Figure 1 of Reference 2.

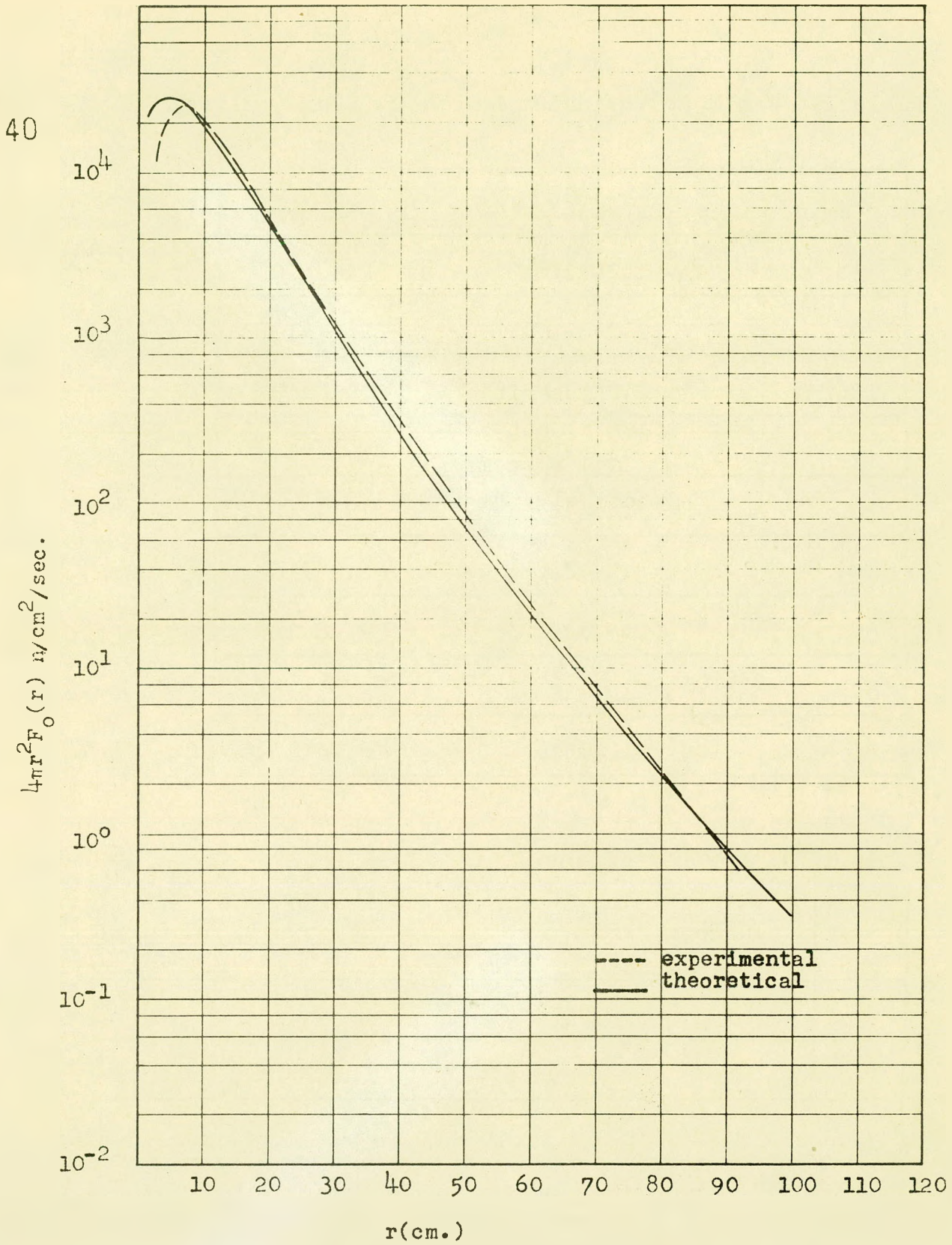

Fig. 1--Indium resonance flux.

Table I. $4\pi r^2 F_o(r)$. Indium Resonance Flux (multiplied by $4\pi r^2$).

r(cm.)	Experiment	Theory
3	1.20×10^{4}	2.48×10^{4}
5	2.27×10^{4}	2.74×10^{4}
10	2.20×10^{4}	1.96×10^{4}
20	5.12×10^{3}	5.12×10^{3}
30	1.16×10^{3}	1.11×10^{3}
40	3.29×10^{2}	2.89×10^{2}
60	2.33×10^{1}	2.08×10^{1}
80	2.30×10^{0}	2.24×10^{0}
90	7.34×10^{-1}	8.26×10^{-1}

Table II. Moments of the Flux.

n	$\overline{r^n}_{exp}$	$\overline{r^n}_{theor}$	$\left(\overline{r^n}\right)^{1/n}_{exp}$ cm	$\left(\overline{r^n}\right)^{1/n}_{theor}$ cm
0	1	1	1	1
2	185	154	13.6	12.4
4	1.222×10^{5}	$.979 \times 10^{5}$	18.7	17.7
6	2.270×10^{8}	1.934×10^{8}	24.7	24.1
8	8.642×10^{11}	8.753×10^{11}	31.5	31.4

Comparisons are made in Table II for $\overline{r^{2n}}$ and for $(\overline{r^{2n}})^{1/2n}$ The significant comparison, that between the $(\overline{r^{2n}})^{1/2n}$, shows good to excellent agreement. The agreement improves with n as far as the comparison is carried, though the near-identity of the values of $\overline{r^8}$ is probably fortuitous.

The one important difference in Table II between the experimental and theoretical results is for $\overline{r^2}$. The theoretical results given here agree well with those obtained by a different method by Zweifel.[3] It is difficult to see how any possible improvement in the theory could bring it significantly closer to experiment. A critical examination of the experimental procedure, especially for the flux at small penetrations, might be worthwhile.

In the present calculation energy degradation on scattering by oxygen was ignored. The high energy flux is depressed somewhat if degradation is included. At fairly large penetrations the low energy (e.g., indium resonance) flux is proportional to the high energy flux and hence is also decreased. While the inclusion of degradation might take care of the very small difference in the slopes of the experimental and theoretical flux curves at large penetrations, it is not in the right direction to improve agreement on r^2.

Appendix I

Data

In order to calculate neutron penetration in water one needs to know the total cross section and the differential scattering cross section of neutrons on hydrogen and oxygen.

At the energies of interest (2 ev - 18 Mev) every n-p collision is a scattering event isotropic in the center-of-mass system.

The parameters describing scattering by oxygen are the scattering cross section σ_{os} and the Legendre coefficients f_ℓ of the angular distribution. If $\sigma(\theta)$ is the differential cross section for scattering through an angle θ in the center-of-mass system,

$$f_\ell = \int_{4\pi} \frac{\sigma(\theta)}{\sigma_{os}} P_\ell(\cos\theta)\, d\Omega_c,$$

where $d\Omega_c$ is the element of solid angle in the center-of-mass system. The normalization is such that $f_o \equiv 1$.

The total hydrogen cross section was taken from an enlarged graph of the data in AECU-2040, Neutron Cross Sections, and is tabulated in Table III.

The absorption cross section for oxygen is negligible below 2.97 Mev and from there on down the scattering cross section σ_{os} is taken equal to the total cross section σ_{oT}. Further, σ_{oT} is taken to have the constant value of 3.8 barns below 330 kev. The oxygen data used for energies of 330 kev and above have previously been published;[4] the data used below 330 kev are given in Table IV.

For energies below 44.7 kev the angular distribution for oxygen is assumed to be isotropic, so that $f_\ell = 0$ when $\ell > 0$.

Table III. Microscopic Cross Sections for Hydrogen

E(Mev)	σ_H(b)	E(Mev)	σ_H(b)	E(kev)	σ_H(b)
18.02	.520	3.13	2.28	544.	6.34
17.14	.550	2.98	2.35	518.	6.51
16.30	.580	2.83	2.43	492.	6.68
15.51	.611	2.69	2.51	468.	6.85
14.75	.648	2.56	2.59	445.	7.00
14.03	.682	2.44	2.66	424.	7.15
13.35	.720	2.32	2.75	403.	7.33
12.70	.760	2.21	2.83	383.	7.50
12.08	.798	2.10	2.91	365.	7.68
11.49	.839	2.00	2.99	347	7.86
10.93	.878	1.90	3.09	330.	8.04
10.40	.920	1.81	3.18	314.	8.20
9.89	.967	1.72	3.28	299.	8.41
9.41	1.01	1.63	3.38	284.	8.63
8.95	1.06	1.55	3.48	270.	8.85
8.51	1.11	1.48	3.58	257.	9.05
8.10	1.16	1.41	3.69	244.	9.26
7.70	1.21	1.34	3.80	233.	9.48
7.33	1.26	1.27	3.91	221.	9.70
6.97	1.31	1.21	4.02	210.	9.90
6.63	1.36	1.15	4.14	200.	10.10
6.30	1.41	1.10	4.27	190.	10.30
6.00	1.47	1.04	4.39	181.	10.51
5.70	1.52	.991	4.53	172.	10.72
5.43	1.58	.943	4.66	164.	10.93
5.16	1.63	.897	4.80	156.	11.15
4.91	1.69	.853	4.94	148.	11.33
4.67	1.75	.812	5.09	141.	11.55
4.44	1.81	.772	5.24	134.	11.75
4.23	1.88	.734	5.40	128.	11.95
4.02	1.94	.699	5.54	121.	12.15
3.82	2.00	.664	5.70	115.	12.36
3.64	2.07	.632	5.86	110.	12.55
3.46	2.13	.601	6.02	104.	12.76
3.29	2.21	.572	6.18	99.4	12.95

E(kev)	σ_H(b)
94.5	13.16
89.9	13.35
85.5	13.55
81.4	13.75
77.4	13.95
73.6	14.15
70.0	14.35
66.6	14.55
63.4	14.75
60.3	14.95
57.3	15.15
54.5	15.32
51.9	15.50
49.4	15.70
47.0	15.90
44.7	16.05
34.8	17.00
27.1	17.70
21.1	18.49
16.4	19.41
12.8	19.90
9.97	20.00
7.76	20.00
6.04	20.00
4.71	20.00
3.67	20.00
2.86	20.00
2.22	20.00
1.73	20.00
1.35	20.00

E(ev)	σ_H(b)
1050.	20.00
818.	20.00
637.	20.00
496.	20.00
386.	20.00
301.	20.00
234.	20.00
183.	20.00
142.	20.00
111.	20.00
86.2	20.00
67.1	20.00
52.3	20.00
40.7	20.00
31.7	20.00
24.7	20.00
19.2	20.00
15.0	20.00
11.7	20.00
9.09	20.00
7.08	20.00
5.51	20.00
4.29	20.00
3.34	20.71
2.60	21.00
2.03	21.00

Table IV. Oxygen Data

E(kev)	σ_{os}(b)	f_1	f_2	f_3
314	3.801	-.392	.0518	.00865
299	3.808	-.352	.0440	.00883
284	3.804	-.324	.0406	.00904
270	3.796	-.299	.0369	.00465
257	3.798	-.284	.0332	.00472
244	3.843	-.267	.0333	.00952
233	3.794	-.265	.0294	.00492
221	3.797	-.255	.0200	.0050
210	3.802	-.236	.0205	.0103
200	3.804	-.230	.0210	.00527
190	3.800	-.229	.0160	.00533
181	3.808	-.224	.0219	.00548
172	3.799	-.210	.0166	.00551
164	3.800	-.199	.0170	.00567
156	3.807	-.190	.0174	.00580
148	3.807	-.182	.0176	.00580
141	3.794	-.188	.0182	
134	3.805	-.177	.0183	
128	3.808	-.169	.0188	
121	3.808	-.165	.0190	
115	3.792	-.170	.0130	
110	3.800	-.164	.0197	
104	3.800	-.154	.0198	
99.4	3.811	-.143	.0136	
94.5	3.798	-.147	.00690	
89.9	3.804	-.141	.00703	
85.5	3.807	-.135	.00707	
81.4	3.796	-.145		
77.4	3.794	-.140		
73.6	3.806	-.133		
70.0	3.801	-.129		
66.6	3.799	-.130		
63.4	3.792	-.124		
60.3	3.797	-.126		
57.3	3.794	-.127		
54.5	3.808	-.113		
51.9	3.814	-.106		
49.4	3.813	-.099		
47.0	3.797	-.101		
44.7	3.789	-.102		

Appendix II

Method of Calculation

The Boltzmann equation for the number flux per unit lethargy range $N(x,u,\omega)$ from a plane isotropic source of fission neutrons in water was converted into a system of coupled integral equations by the method of moments.*[5,6] Here

x = penetration

$u = \ell n\ (E/0.33)$ = lethargy, E given in Mev

ω = direction cosine of neutron motion with normal to source plane.

The simplifying assumption was made that oxygen behaves like an infinitely heavy scatterer.**[5] The center-of-mass system and the laboratory system then become identical and the neutron energy does not change on collision.

We define

$\sigma_H(u)$ = microscopic cross section of hydrogen in barns,

$\Sigma_H(u) = (.602/9)\ \sigma_H(u)$ = macroscopic cross section of hydrogen in cm^{-1},

$S(E) = \sqrt{\frac{2}{\pi e}}\ e^{-E} \sinh \sqrt{2E}$ = Watt's fission spectrum, neutrons per Mev per fission neutron,

$g(u) = S(E)/E$,

$\sigma_{oT}(u)$ = total microscopic oxygen cross section in barns,

$$A_\ell(u) = 1 + \frac{\sigma_{oT}(u) - \sigma_{os} f_\ell(u)}{2\sigma_H(u)}\ ;\ ***$$

---

* Cf. (5), equations (12) and (38). Reference 6 gives the equation for the photon case.

** Cf. (5), equation (14).

*** The angular distribution $f(u,\mu) = \sigma(\theta)/\sigma_{os}$ can be reconstructed from its Legendre coefficients f_ℓ as the sum

$$f(u,\mu) = \sum_{\ell=0}^{\infty} \frac{2\ell+1}{4\pi} f_\ell(u)\ P_\ell(\mu)$$

a_o = normalizing factor chosen to facilitate machine computation.

The modified moments $D_{n\ell}(u)$, defined by the relation

$$D_{n\ell} = e^{-u} \Sigma_H(u) \int_{-\infty}^{\infty} \frac{(a_o x)^n}{n!} d(a_o x) \int_{\pi} N(x,u,\omega) P_\ell(\omega) \, d\Omega,$$

satisfy the set of equations *

$$A_\ell(u) D_{n\ell}(u) = \int_u^4 P_\ell(e^{\frac{u-u'}{2}}) D_{n\ell}(u') du'$$

$$+ \frac{a_o}{\Sigma_H(u)} \left[\frac{(\ell+1) D_{n-1,\ell+1}(u) + \ell D_{n-1,\ell-1}(u)}{2\ell + 1} \right]$$

$$+ a_o e^{-u} g(u) \delta_{no} \delta_{\ell o}, \quad **$$

where δ_{no} is the Kronecker delta.

The set of equations for the $D_{n\ell}$ was coded for SEAC (Standard Eastern Automatic Computer) by Mr. Norman Levine. By use of the standard memory it was possible to carry out the integration down to 44.7 kev in steps which were small enough so that the resonances in the oxygen cross section and the variations in the $f_\ell(u)$ were adequately represented. In order to carry the integration down to the electron volt range, a major revision of the code was

---

* Cf. (5), equation (43). The source terms are different because equation (43) is for the moments of the scattered flux from a monoenergetic source while the present equation is for the moments of the total flux from a fission source.

** We choose a lethargy of u = 4 (18 Mev) as the upper limit of integration.

required which necessitated the use of the newly available Williams tube memory facility. By careful adjustment of the scaling factors to prevent overflow and at the same time retain significance, the modified moments D_{no},* given in Table V, were obtained for E = 2.03 ev.

Table V. Plane Isotropic Moments

n	D_{no}	$10^{-(n+1)} F^{p\ell}_{no}$
0	17016.	36700.
2	4371.5	9428.5
4	1387.7	2993.0
6	653.01	1408.4
8	410.46	885.27
10	323.43	697.58
12	285.34	615.42
14	272.38	587.47

The averages $\overline{r^{2n}}$ were computed not from the flux but directly from the moments. The $D_{n\ell}(u)$ computed by the machine are the modified moments of the flux given per unit lethargy range. The plane isotropic (2n,0) moments per unit energy range, defined by the relation

$$F^{p\ell}_{2n,o}(E) = \frac{1}{(2n)!}\int_{-\infty}^{\infty} x^n\, dx \int_{4\pi} N(x,u,\omega)\, d\Omega,$$

are, in terms of the $D_{2n,o}(u)$

$$F^{p\ell}_{2n,o}(E) = \frac{D_{2n,o}(u)}{.33\Sigma_H(u)}\, 10^{2n+1},$$

since a_o was chosen to be 0.1.

* All odd moments D_{10}, D_{30}, etc. vanish.

$10^{-(2n+1)}$ times the $F^{pl}_{2n,o}$ at 2.03 ev are given in Table V along with the $D_{2n,o}$.

The moments $F_{2n,o}(E)$ of the point isotropic flux are defined by the relation

$$F_{2n,o}(E) = \frac{1}{(2n)!}\int_o^\infty r^{2n}\, 4\pi r^2\, F_o(r,E)\, dr,$$

where $F_o(r,E)$ is the flux per unit energy range at r with energy E from a point isotropic source. The $F_{2n,o}$ are in terms of the plane isotropic moments,

$$F_{2n,o} = (2n+1)\, F^{pl}_{2n,o} \quad (7).$$

The averages $\overline{r^{2n}}$ are given by

$$\overline{r^{2n}} = \frac{(2n)!\, F_{2n,o}}{F_{o,o}} \quad \left(= (2n+1)!\, 10^{2n}\, \frac{D_{2n,o}}{D_{o,o}} \right).$$

Since the behavior of the flux (rather, $4\pi r^2$ times the flux) at large distances is nearly exponential and since the scattered radiation vanishes at r = 0, a linear combination of functions of the form re^{-ar} was used to reconstruct the scattered contribution to the point isotropic function $4\pi r^2 F_o(r)$ from the computed plane isotropic moments. The actual fit used was

$$4\pi r^2 F_o(r) = 9.7\times10^{-4}\, e^{-1.53r} + r\left[155.2e^{-.1126r} + 15207e^{-.2075r}\right], \quad 0 \leq r \leq 25 \text{ cm}$$

$$= 1110, \quad r = 30 \text{ cm}$$

$$= r\left[89.36e^{-.1030r} + 7554.1e^{-.1795r}\right], \quad r > 35 \text{ cm}$$

Between 25 and 35 cm $4\pi r^2 F_o(r)$ was found by interpolation. The first term in the expression used for $r \leq 25$ cm is the unscattered flux.

One can recompute the $F^{p\ell}_{2n,o}$ from the expressions given here for $4\pi r^2 F_o(r)$. The agreement with the plane isotropic moments obtained from the machine computation is closer than one percent.

A general discussion of the techniques used for fitting the flux from the moments will be contained in a forthcoming report.

40

References

(1) J. Hill, L. Roberts, and T. Fitch, ORNL 181, December 1948.
(2) P. Zweifel, address at Shielding Information Meeting, May 13-14, 1954.
(3) H. Goldstein and J. Certaine, NDA 15C-36, May 1954.
(4) H. Goldstein, NDA 15C-15, Fast Neutron Data for Oxygen, November 1953.
(5) J. Certaine, NDA 15C-12, Integral Term for Elastic Scattering of Particles, July 1953.
(6) L. Spencer and U. Fano, J. Res. NBS 46, 446 (1951).
(7) H. Goldstein, J.E. Wilkins, Jr., and S. Preiser, NDA 15C-20, Interim Report on the NDA-NBS Calculations of Gamma Ray Penetration, September 1953.